JACS
JOURNAL OF THE AMERICAN CHEMICAL SOCIETY
Article
pubs.acs.org/JACS

Induction of Thermotropic Bicontinuous Cubic Phases in Liquid-Crystalline Ammonium and Phosphonium Salts

Takahiro Ichikawa,[†,‡] Masafumi Yoshio,[†] Atsushi Hamasaki,[‡] Satomi Taguchi,[‡] Feng Liu,[§] Xiang-bing Zeng,[§] Goran Ungar,[§,∥] Hiroyuki Ohno,[‡] and Takashi Kato*[,†]

[†]Department of Chemistry and Biotechnology, School of Engineering, The University of Tokyo, Hongo, Bunkyo-ku, Tokyo 113-8656, Japan

[‡]Department of Biotechnology, Tokyo University of Agriculture and Technology, Nakacho, Koganei, Tokyo 184-8588, Japan

[§]Department of Materials Science and Engineering, University of Sheffield, Mappin Street, Sheffield S1 3JD, United Kingdom

[∥]WCU Program C_2E_2, School of Chemical and Biological Engineering, Seoul National University, Seoul, South Korea

Supporting Information

ABSTRACT: Two series of wedge-shaped onium salts, one ammonium and the other phosphonium, having 3,4,5-tris(alkyloxy)benzyl moieties, exhibit thermotropic bicontinuous "gyroid" cubic (Cub_{bi}) and hexagonal columnar liquid-crystalline (LC) phases by nanosegregation between ionophilic and ionophobic parts. The alkyl chain lengths on the cationic moieties, anion species, and alkyl chain lengths on the benzyl moieties have crucial effects on their thermotropic phase behavior. For example, triethyl-[3,4,5-tris(dodecyloxy)benzyl]-ammonium hexafluorophosphate forms the thermotropic $Ia\bar{3}d$ Cub_{bi} LC phase, whereas an analogous compound with trifluoromethanesulfonate anion shows no LC properties. Synchrotron small-angle diffraction intensities from the $Ia\bar{3}d$ Cub_{bi} LC materials provide electron density maps in the bulk state. The resulting maps show convincingly that the $Ia\bar{3}d$ Cub_{bi} structure is composed of three-dimensionally interconnected ion nanochannel networks surrounded by aliphatic domains. A novel differential mapping technique has been applied successfully. The map of triethyl-[3,4,5-tris(decyloxy)benzyl]ammonium tetrafluoroborate has been subtracted from that of the analogous ammonium salt with hexafluorophosphate anion in the $Ia\bar{3}d$ Cub_{bi} phases. The differential map shows that the counteranions are located in the core of the three-dimensionally interconnected nanochannel networks. Changing from trimethyl- via triethyl- to tripropylammonium cation changes the phase from columnar to Cub_{bi} to no mesophase, respectively. This sensitivity to the widened shape for the narrow end of the molecule is explained successfully by the previously proposed semiquantitative geometric model based on the radial distribution of volume in wedge-shaped molecules. The LC onium salts dissolve lithium tetrafluoroborate without losing the $Ia\bar{3}d$ Cub_{bi} LC phase. The Cub_{bi} LC materials exhibit efficient ion-transporting behavior as a result of their 3D interconnected ion nanochannel networks. The $Ia\bar{3}d$ Cub_{bi} LC material formed by triethyl-[3,4,5-tris(decyloxy)benzyl]phosphonium tetrafluoroborate shows ionic conductivities higher than the analogous $Ia\bar{3}d$ Cub_{bi} material based on ammonium salts. The present study indicates great potential of Cub_{bi} LC nanostructures consisting of ionic molecules for development of transportation nanochannel materials.

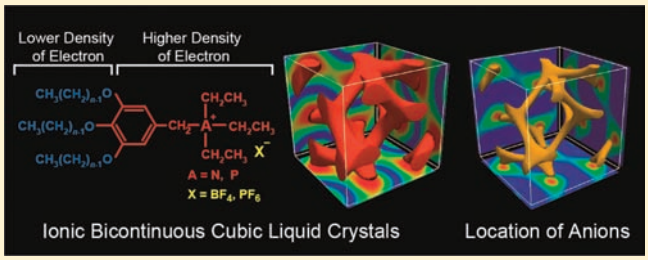

INTRODUCTION

Bicontinuous cubic (Cub_{bi}) phases[1] are a group of nanostructured liquid-crystalline (LC) phases having three-dimensionally (3D) interconnected nanochannels.[2−4] Recently, Cub_{bi} liquid crystals have attracted attention as transportation materials[5−11] because the 3D channels of Cub_{bi} LC materials are expected to form successive pathways without the orientation of the liquid-crystal domains, while decades of studies have mainly focused only on the molecular assembled structures in the Cub_{bi} phases.[2−4] As an example for application to transportation materials, we previously succeeded in development of ion-conductive materials formed by Cub_{bi} LC ionic compounds.[6−8] Since the channel structures of Cub_{bi} LC materials possess well-defined sizes and shapes, there are great expectations for their application in nanofiltration membranes[9,10] and drug delivery systems.[12]

There are a limited number of reports on the application of Cub_{bi} LC materials.[5−14] Focusing only on thermotropic Cub_{bi} LC systems, the number is further limited.[6−8,14] This is due to the difficulty in designing LC molecules that would exhibit thermotropic Cub_{bi} phases. For the design of LC materials, it is generally thought that control of intermolecular interactions, such as hydrogen bonding, electrostatic interaction, van der Waals interaction, and $\pi-\pi$ interaction, is important.[15−19] On the basis of this idea, a number of new functional LC materials

Received: September 25, 2011
Published: January 9, 2012

   dx.doi.org/10.1021/ja209010m | J. Am. Chem.Soc. 2012, 134, 2634−2643

have been developed and the relationships between the molecular structure and the molecular assembled nanostructures have been studied.[20−26] There has been some progress in rational design of thermotropic LC molecules intended to exhibit nematic, smectic, and columnar phases by accumulation of data on structure/property relationships. However, it is still difficult to design LC molecules exhibiting thermotropic Cub_{bi} phases. Therefore, more study is required to obtain Cub_{bi} LC materials, which have considerable potential as functional nanochannel materials.

Our intention is to gain further insights into the design of thermotropic Cub_{bi} liquid crystals and evaluate them as potential transportation materials. In our previous study we prepared a variety of ionic compounds showing thermotropic LC properties for development of a new type of ion-conducting material.[6,7,17,20] In the course of our study on ionic LC molecules, we found that wedge-shaped ammonium salts form thermotropic $Ia\bar{3}d$ Cub_{bi} phases.[6] Moreover, we succeeded in the preparation of polymer films having 3D ion nanochannels through in situ photopolymerization of a Cub_{bi} LC ammonium salt having a polymerizable group.[7] On the basis of our previous results on the ionic compounds showing Cub_{bi} phases, we focused on the wedge-shaped onium structures consisting of ionophobic and ionophilic parts as a promising design for Cub_{bi} LC molecules (Figure 1). Though there have been a lot of

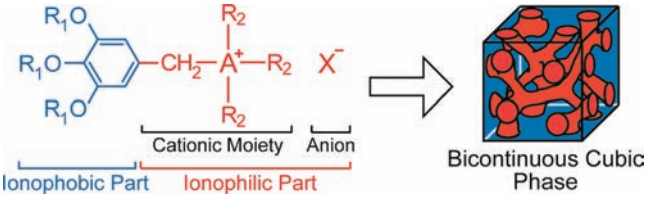

Figure 1. Molecular design in this work for development of thermotropic liquid-crystalline material forming bicontinuous cubic phases.

reports on the LC molecules containing ionic moieties,[17,20,27] induction of Cub_{bi} phases has been observed only in a handful of ionic compounds[4a,b,28] including our previously reported molecules.[6,7]

In the present study, we prepared two series of wedge-shaped ammonium salts **1**−**3** and phosphonium salts **4**−**6** (Figure 2)

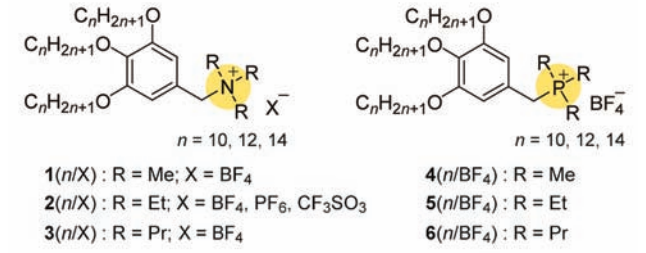

Figure 2. Molecular structures of wedge-shaped ammonium salts **1**−**3**(n/X) and phosphonium salts **4**−**6**(n/BF_4).

to examine the effects of the cationic moieties, alkyl chain length n, and anion species on their LC properties. We focused on induction of Cub_{bi} phases. Since phosphonium salts have similar properties to ammonium salts, they have been studied for comparison with ammonium salts.[29] For example, phosphonium cations have been recently used as alternatives to ammonium cations for design of ionic liquids.[30−32] Phosphonium-based ionic liquids generally exhibit more chemical and thermal stability than the corresponding ammonium-based ionic liquids.[31] Moreover, they show higher ionic conductivity than the corresponding ammonium salts.[32] On the other hand, there have been several reports on phosphonium salts with LC properties.[33,34] For example, Weiss et al. reported the LC behavior of quaternary phosphonium salts having two or three long alkyl chains.[34] They revealed that the LC phosphonium salts form molecular assembled structures similar to the analogous ammonium salts. With this background in mind, we expected that introduction of phosphonium structures into our material design would result in an improvement of the Cub_{bi} LC materials. We also expected that comparison of the LC behavior of **1**−**3**(n/BF_4) with that of **4**−**6**(n/BF_4) would improve our knowledge of the design of thermotropic Cub_{bi} LC molecules.

RESULTS AND DISCUSSION

Ionic/Nonionic Bicontinuous Cubic Structures Formed by 2(10/BF_4) and 2(10/PF_6). In our preliminary communication,[6] the LC behavior of compounds **2**(n/BF_4) (n = 10, 12, 14) was reported. We revealed that compounds **2**(n/BF_4) having a triethyl ammonium moiety form Cub_{bi} phases, space group $Ia\bar{3}d$, depending on the alkyl chain length n. For example, compound **2**$(10/BF_4)$ exhibits a Cub_{bi} phase from 61 to −32 °C on cooling.[6]

To examine the effects of ionic structures on formation of the Cub_{bi} phase, we prepared an analogous compound **2**$(10/PF_6)$ with an anion different than that in **2**$(10/BF_4)$. Compound **2**$(10/PF_6)$ shows a Cub_{bi} LC phase from 34 to −45 °C on cooling. The detailed LC behavior of **2**$(10/PF_6)$ will be discussed further below. We expected that comparison of the molecular assembly of **2**$(10/BF_4)$ and **2**$(10/PF_6)$ would provide new insight into the Cub_{bi} structures. Synchrotron small-angle diffraction experiments were performed on compounds **2**$(10/BF_4)$ and **2**$(10/PF_6)$. These experiments enabled reconstruction of electron density maps of the Cub_{bi} phases in the bulk state. Figure 3a shows the map of a unit cell of the $Ia\bar{3}d$ Cub_{bi} phase in **2**$(10/BF_4)$. The high electron density (orange) and the low density (blue) regions represent, respectively, aromatic/ionic and aliphatic domains rich in chain ends. The high-density regions form the two continuous antichiral channel networks; the two networks are separated by a low-density sheath (blue) that follows the gyroid G-surface of minimum curvature. Figure 3b is the map of **2**$(10/PF_6)$ from which the map of **2**$(10/BF_4)$ had been subtracted. Prior to subtraction the maps had been scaled based on electron density histograms.[35] The difference between the two maps is caused by the extra electrons contained in PF_6 as compared to BF_4. The yellow isoelectron surface in Figure 3b encloses the regions where the maps differ most, i.e., the regions richest in anions; for details see the Supporting Information. These results provide compelling evidence that the ionophilic parts occupy the 3D networks of interconnected channels in the $Ia\bar{3}d$ Cub_{bi} structure. It is considered that the localization of anions in the nanosegregated structures is important in the design of ion-transporting and nanochannel materials.

Effects of Cationic Moieties of Wedge-Shaped Ammonium Salts on Mesomorphism. To examine the effects of the molecular structures of ammonium compounds **2**(n/BF_4) on induction of $Ia\bar{3}d$ Cub_{bi} phases, we designed and synthesized analogous ammonium salts **1**(n/BF_4) and

dx.doi.org/10.1021/ja209010m | J. Am. Chem.Soc. 2012, 134, 2634−2643

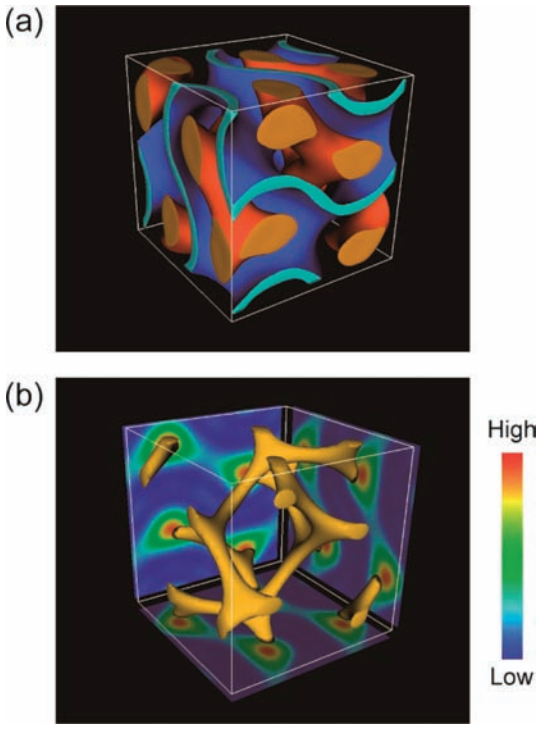

Figure 3. (a) Electron density map ρ obtained from small-angle diffraction intensities of a powder pattern of **2**(10/BF_4) in the $Ia\bar{3}d$ Cub_{bi} phase at 20 °C. High-density regions (aromatic/ionic) are enclosed within the orange isoelectron surfaces and low-density regions (alkyl chain ends) within the blue surfaces. (b) Differential electron density map $\rho\{$**2**(10/PF_6)$\}$ − $\rho\{$(**2**(10/BF_4)$\}$, showing the preferred location of anions enclosed within the yellow isosurfaces. 2D maps lining the walls of b are cuts in (100), (010), and (001) planes; refer to the color scale on the right.

3(n/BF_4) having different cationic moieties from **2**(n/BF_4). The thermal properties of ammonium salts **1**−**3**(n/BF_4) are presented in Table 1. The thermal properties of these ammonium salts differ significantly between the compounds, depending on the structures of the cationic moiety.

Compounds **1**(n/BF_4), having a trimethyl ammonium moiety, which is smaller than that of **2**(n/BF_4), form hexagonal columnar phases. Figure 4 shows a typical XRD pattern of **1**(12/BF_4) in the Col_h phase at 150 °C. The intense peak at 30.2 Å and the two weak peaks at 17.5 and 15.2 Å are observed with the reciprocal d-spacing ratio of 1:$\sqrt{3}$:2, which can be

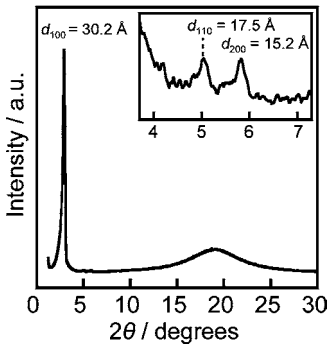

Figure 4. Wide-angle X-ray diffraction pattern of **1**(12/BF_4) in the Col_h phase at 150 °C.

indexed as the (10), (11), and (20) reflections of the 2D hexagonal arrangement of the columns. The Col_h mesophases formed by compounds **1**(n/BF_4) are stable up to about 200 °C, whereas **2**(n/BF_4) exhibits isotropization below 150 °C. The higher isotropization temperatures of **1**(n/BF_4) are partly attributed to stronger electrostatic interactions between the smaller cationic moiety and the anion in the ionic domain, but partly it is believed to be the result of a better match between the geometry of the molecule and that of the space available to it in the particular LC phase (see below).

In contrast, compounds **3**(n/BF_4), having a tripropyl ammonium moiety, which is larger than that of **2**(n/BF_4), show no mesomorphic properties except for **3**(14/BF_4). It is likely that mesophase formation is disfavored partially by the fact that the bulky tripropyl ammonium moiety sterically hinders the counteranion from interacting closely with the cationic moiety in the ionic domain. Furthermore, increasing nanosegregation may be partly responsible for the fact that extending the alkyl chain n beyond 14 induces formation of the mesophase, e.g., **3**(14/BF_4) shows a columnar phase between 80 and 91 °C. However, a single unified geometry-based scheme is capable of explaining, at least qualitatively, most features of the observed phase behavior of compounds in this study.

The geometric scheme was originally devised to rationalize the fact that different wedge-shaped molecules, such as dendrons, form different 3D-ordered LC phases (cubic, tetragonal) consisting of spherical clusters and to explain thermotropic polymorphism in such compounds.[18h] The principle was later extended to bicontinuous and tricontinuous

Table 1. Thermal Properties of Ammonium Compounds 1−3(n/BF_4)

		phase transition behavior[a]						
compound	n							
1(n/BF_4)	10	Cr	60 (8.0)	Col_h	194[b] (−)[c]	Iso		
	12	Cr	44 (27)	Cr	60 (9.1)	Col_h	206[b] (−)[c]	Iso
	14	Cr	57 (77)	Col_h	202[b] (−)[c]	Iso		
2(n/BF_4)	10[d]	Cr	42 (0.44)	Cub_{bi}	82 (0.83)	Iso		
	12[d]	Cr	32 (29)	Cub_{bi}	49 (0.80)	Col_h	126 (0.63)	Iso
	14[d]	Cr	53 (63)	Col_h	142 (0.99)	Iso		
3(n/BF_4)	10	Cr	82 (28)	Iso				
	12	Cr	80 (31)	Iso				
	14	Cr	80 (26)	Col_h	91 (0.82)	Iso		

[a]Cr, crystalline; Cub_{bi}, bicontinuous cubic; Col_h, hexagonal columnar; Iso, isotropic. Transition temperatures (°C) and enthalpy changes (kJ mol^{-1}, in parentheses) are determined by DSC on the second heating. [b]Transitions are determined by visual observation with a polarizing optical microscope. [c]No transition enthalpy was detected by the DSC. [d]Reference 7.

dx.doi.org/10.1021/ja209010m | J. Am. Chem.Soc. 2012, 134, 2634−2643

cubic phases.[2c] A bicontinuous cubic, such as $Ia\bar{3}d$, can be represented by networks of branching cylindrical rods (Figure 3). As shown above, the ionic groups, i.e., the narrow ends of the wedge-shaped molecules, are located near the central axis of the cylinders. In order to determine the ideal shape of a molecule that would fit perfectly into a given mesophase, we start at the central cylinder axis and calculate the rate of increase in volume of the cylinder network, dV/dr, as the radius r is increased. The result for the $Ia\bar{3}d$ Cub_{bi} phase is shown in Figure 5 (full line), together with the results for the hexagonal

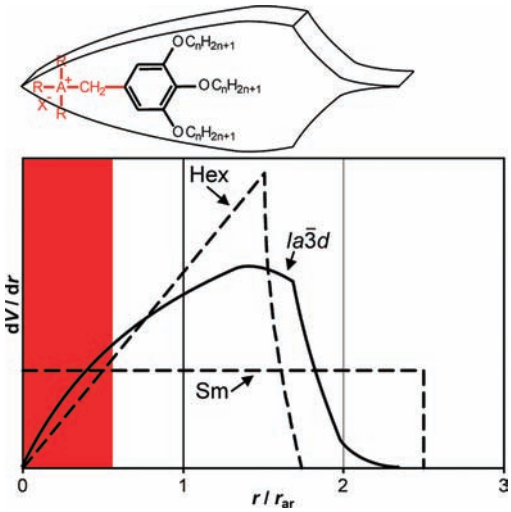

Figure 5. dV/dr plots for three LC phases: Col_h (Hex), smectic (Sm), and bicontinuous cubic ($Ia\bar{3}d$). (Top) Schematic drawing of the molecular cross-section area profile, $A(r)$, which should match dV/dr for uniform filling of the volume of a particular phase. Curves are scaled horizontally to the same radius r_{ar} delimiting the "aromatic" volume fraction (including all but the peripheral alkoxy chains) from the alkoxy fraction. Vertical scaling normalizes the areas under the curves.

columnar phase and the smectic (layered) phase with the molecular axis normal to the layers (dashed lines). For the Col_h phase the cylinders grow in radius unhindered, with $dV/dr \propto r$, until the parallel cylinders clash (around $r = 1.5$ in Figure 5). As further growth in volume takes place only where the cylinders do not overlap, dV/dr drops sharply and falls to 0 when all space is filled. Thus, the ideal shape of a molecule to fit into the Col_h phase is one for which the cross-sectional area increases linearly, i.e., $A(r) \propto dV/dr \propto r$, and then drops quite abruptly to zero (dashed curve in Figure 5). At the other extreme are molecules that are not tapered at all but maintain a constant A throughout, i.e., where $A(r) \propto dV/dr \propto r^0 = 1$ (dashed rectangle). Molecules whose shape can be described by a fractional exponent, i.e., where $A(r) \propto dV/dr \propto r^m$, with $0 < m < 1$, are likely to form a bicontinuous or tricontinuous cubic phase. Which of the phase variants will actually appear is determined by the precise shape of the molecule in its most probable conformation.[2c]

We can see now why on going from compound **1**$(12/BF_4)$ to **2**$(12/BF_4)$, i.e., by replacing the trimethyl with the triethyl ammonium group, the structure changes from Col_h to $Ia\bar{3}d$ Cub_{bi}; close to $r = 0$ the $A(r)$ curve for the $Ia\bar{3}d$ Cub_{bi} phase is higher than the curve for the Col_h phase. The extra cross-section near the apex of the molecule is provided by the three extra methylene groups. By the same reasoning one might expect that moving to compound **3**$(12/BF_4)$ we might get the smectic phase. However, this compound does not form a mesophase. Presumably the equilibrium shape of the **3**$(12/BF_4)$ molecule does not match sufficiently closely to any of the curves in Figure 5, and if the length of the alkyls in the ammonium moiety were increased further, perhaps a smectic phase would form. However, the fact that compound **3**$(14/BF_4)$ forms the Col_h phase at higher temperatures suggests that the extra six methylenes at the outer end (large r) tips the distribution of volume back to the right in Figure 5, sufficiently close to the Col_h (Hex) curve.

These results suggest that the design of the size and shape of the narrow end of the series of wedge-shaped ammonium salts is particularly important in directing the type of their mesophase assembly. This is in agreement with the previous finding that small changes at the narrow end of wedge-shaped molecules have a disproportionally large effect on the phase morphology in 3D LC phases of spherical aggregates.[36] The above geometric model has shown once again its usefulness in relating molecular architecture to the morphology of the mesophase.

Comparison of the Mesomorphic Properties of Ammonium and Phosphonium Wedge-Shaped Salts. The thermal properties of phosphonium salts **4**–**6**(n/BF_4) are presented in Table 2. It is of interest to compare the LC properties of these phosphonium salts with those of the corresponding ammonium salts **1**–**3**(n/BF_4). Phosphonium compounds **4**(n/BF_4), having a triethyl phosphonium moiety, form Col_h phases, just as in the corresponding ammonium compounds **1**(n/BF_4). For the series of **4**(n/BF_4), the

Table 2. Thermal Properties of Phosphonium Compounds 4–6(n/BF_4)

		phase transition behavior[a]						
compound	n							
4(n/BF_4)	10	Cr	55 (8.3)	Col_h	164 (0.88)	Iso		
	12	Cr	6 (14)	Cr	34 (3.7)	Col_h	181 (0.70)	Iso
	14	Cr	40 (29)	Col_h	164 (0.55)	Iso		
5(n/BF_4)	10	Cr	−17 (16)	Cr	0 (18)	Cub_{bi}	48 (0.76)	Iso
	12	Cr	31 (43)	Col_h	102 (0.63)	Iso		
	14	Cr	50 (59)	Col_h	127 (0.53)	Iso		
6(n/BF_4)	10	Cr	31 (26)	Col_h	66 (3.5)	Iso		
	12	Cr	37 (44)	Cr	62 (23)	Col_h	88 (2.5)	Iso
	14	Cr	39 (45)	Cr	64 (29)	Col_h	93 (1.2)	Iso

[a]Cr, crystalline; Cub_{bi}, bicontinuous cubic; Col_h, hexagonal columnar; Iso, isotropic. Transition temperatures (°C) and enthalpy changes (kJ mol^{-1}, in parentheses) are determined by DSC on the second heating.

dx.doi.org/10.1021/ja209010m | J. Am. Chem.Soc. 2012, 134, 2634–2643

isotropization temperatures are lower than those for the $\mathbf{1}(n/BF_4)$ series. This behavior can be explained by the weakening of electrostatic interactions as the cation atom changes from nitrogen to phosphorus. This assumption is further supported by the comparison of the isotropization temperatures of ammonium salts **2**, $\mathbf{3}(n/BF_4)$ and phosphonium salts **5**, $\mathbf{6}(n/BF_4)$.

Induction of Cub_{bi} phase is observed for phosphonium compound $\mathbf{5}(10/BF_4)$, having a triethyl onium moiety, as well as the corresponding ammonium compound $\mathbf{2}(10/BF_4)$. Compound $\mathbf{5}(10/BF_4)$ exhibits a Cub_{bi} phase from 0 to 48 °C on heating. Figure 6 shows the small-angle X-ray scattering pattern for $\mathbf{5}(10/BF_4)$ in the Cub_{bi} phase at 35 °C. Two sharp peaks at 32.3 Å and 27.7 Å and four weak peaks at 20.7, 17.5, 16.7, and 15.4 Å are observed. The reciprocal spacing ratio of these six peaks is $\sqrt{6}:\sqrt{8}:\sqrt{14}:\sqrt{20}:\sqrt{22}:\sqrt{26}$; hence, the peaks can be indexed as (211), (220), (321), (420), ($3\bar{3}2$), and (510) reflections of the gyroid Cub_{bi} phase with $Ia\bar{3}d$ symmetry. The lattice parameter (a) of the cubic structure is calculated to be 79 Å, and the number (N) of molecules for the unit cell is estimated to be 4.6×10^2 from $N = N_A a^3 \rho / M$, where N_A is Avogadro's number (6.02×10^{23} mol^{-1}) and M is the molecular weight (764.89 g mol^{-1}). The density (ρ) of the material is 1.2 g cm^{-3}, which has been determined by the floatation method in D-(+)-sucrose/H_2O at 20 °C. The self-assembled nanostructure formed by $\mathbf{5}(10/BF_4)$ has also been examined by synchrotron small-angle diffraction experiments. Comparison of the electron density maps of $\mathbf{5}(10/BF_4)$ with that of $\mathbf{2}(10/BF_4)$ (see Supporting Information) reveals that the self-assembled $Ia\bar{3}d$ Cub_{bi} nanostructures formed by $\mathbf{2}(10/BF_4)$ and $\mathbf{5}(10/BF_4)$ are very similar.

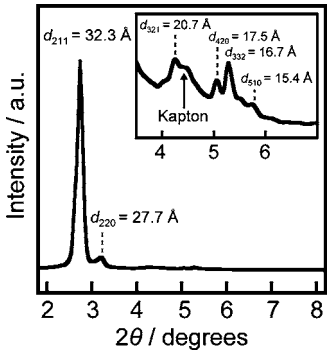

Figure 6. Small-angle X-ray scattering pattern of $\mathbf{5}(10/BF_4)$ in the $Ia\bar{3}d$ Cub_{bi} phase at 35 °C.

Figure 7 compares the thermal properties of ammonium salts $\mathbf{2}(n/BF_4)$ and phosphonium salts $\mathbf{5}(n/BF_4)$ having triethyl onium moieties. It is noteworthy that $\mathbf{2}(n/BF_4)$ and $\mathbf{5}(n/BF_4)$ show similar variation in phase sequence and transition temperatures on alkyl chain length n. For example, only $\mathbf{2}(10/BF_4)$ and $\mathbf{5}(10/BF_4)$ exhibit the single $Ia\bar{3}d$ Cub_{bi} phases which transform directly to the isotropic phases. In addition, it is common to both $\mathbf{2}(n/BF_4)$ and $\mathbf{5}(n/BF_4)$ that increasing the alkyl chain length n leads to induction of Col_h phases. These results suggest that induction of Cub_{bi} phases is very sensitive to the length n of the alkyl chains tethered to the molecules.

In contrast to the similarity in the phase behavior between **1**, $\mathbf{2}(n/BF_4)$, and **4**, $\mathbf{5}(n/BF_4)$, ammonium compounds $\mathbf{3}(n/BF_4)$ and phosphonium compounds $\mathbf{6}(n/BF_4)$, having tripropyl onium moieties, differ considerably in their phase behavior. For example, $\mathbf{6}(10/BF_4)$ forms a Col_h phase from 31 to 66 °C on heating, whereas $\mathbf{3}(10/BF_4)$ exhibits no mesomorphism. Another difference is observed in the enthalpy of isotropization. The enthalpy values of compounds $\mathbf{6}(n/BF_4)$ (n = 10, 12, 14) are 3.5, 2.5, and 1.2 kJ mol^{-1}, which are larger than those of compounds $\mathbf{1}-\mathbf{5}(n/BF_4)$. We attribute the mesophase formation in compounds $\mathbf{6}(n/BF_4)$ to van der Waals interactions between the phosphonium cation moieties. This assumption is consistent with the general tendency of phosphonium salts to form stronger van der Waals interactions compared to the corresponding ammonium salts.[32−34]

The fact that the Cub_{bi} phase is observed only in compound $\mathbf{5}(10/BF_4)$ among the series of phosphonium salts $\mathbf{4}-\mathbf{6}(n/BF_4)$ further supports the conclusion that the triethyl onium moieties play an important role in inducing the Cub_{bi} phase.

^{1}H NMR Studies of Ammonium and Phosphonium Salts. ^{1}H NMR studies of $CDCl_3$ solutions of these salts have been performed in order to compare the ammonium and phosphonium salts with regard to ionicity of the cationic moiety. Figure 8 shows the ^{1}H NMR spectra of compounds $\mathbf{2}(10/BF_4)$ and $\mathbf{5}(10/BF_4)$. A coupling peak corresponding to the benzyl phosphonium proton for $\mathbf{5}(10/BF_4)$ appears at 3.62 ppm (Figure 8b), whereas a corresponding singlet peak for analogous ammonium salt $\mathbf{2}(10/BF_4)$ is observed at 4.30 ppm (Figure 8a). These results suggest that the phosphonium cation

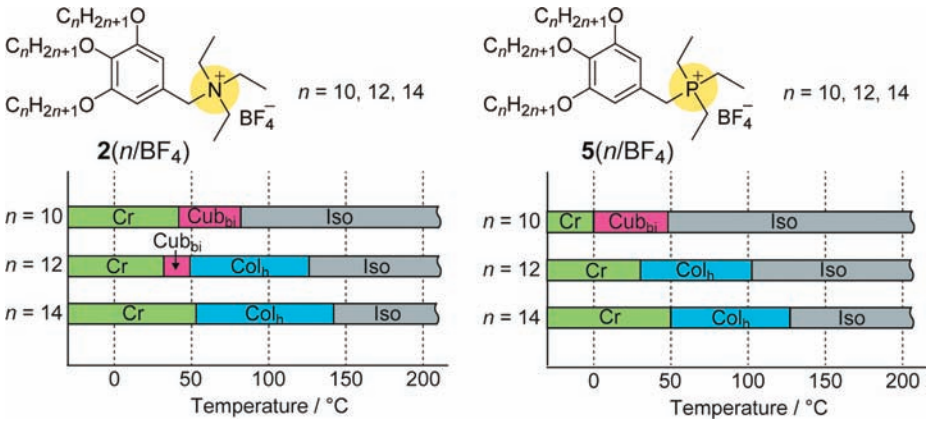

Figure 7. Comparison of LC phase sequences of $\mathbf{2}(n/BF_4)$ and $\mathbf{5}(n/BF_4)$: Cr, crystalline; Cub_{bi}, bicontinuous cubic; Col_h, hexagonal columnar; Iso, isotropic.

dx.doi.org/10.1021/ja209010m | J. Am. Chem.Soc. 2012, 134, 2634−2643

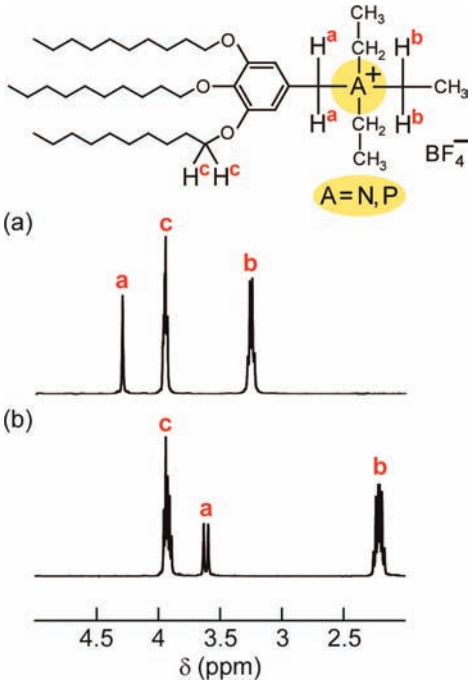

Figure 8. ^{1}H NMR spectra of (a) ammonium-based compound **2**(10/BF_4) and (b) phosphonium-based compound **5**(10/BF_4) in $CDCl_3$ (50 mM) at 20 °C.

is less positively charged than the ammonium cation and therefore forms weaker electrostatic interaction with counteranion. This speculation is consistent with the tendency in the bulk state for the phosphonium compounds **4**–**6**(n/BF_4) to turn isotropic at lower temperatures than the corresponding ammonium compounds **1**–**3**(n/BF_4).

Complexation of the Cub_{bi} LC Salts with Lithium Tetrafluoroborate. One interesting potential application of these ionic nanostructured liquid crystals is their use as electrolytes in lithium batteries.[5] Figure 9 shows our material design for a new class of lithium ion conductors having a Cub_{bi} LC structure. It is important to examine whether the wedge-shaped onium salts show compatibility with lithium salts and form Cub_{bi} phases in the presence of lithium salts. We mixed the wedge-shaped onium salts and lithium tetrafluoroborate ($LiBF_4$) in various ratios. As LC samples, compounds **2**(10/BF_4) and **5**(10/BF_4), which exhibit only the $Ia\bar{3}d$ Cub_{bi} phases, were selected. The mixtures were prepared by slow evaporation of the tetrahydrofuran solution of **2**(10/BF_4) or **5**(10/BF_4) and the requisite amounts of $LiBF_4$.

The LC properties of the mixtures were examined by polarizing optical microscopy, differential scanning calorimetry (DSC), and X-ray diffraction measurements. These mixtures show not only $Ia\bar{3}d$ Cub_{bi} phases but also Col_h phases. For example, upon cooling the isotropic liquid mixture **5**(10/BF_4)/$LiBF_4$ with a 4:1 molar ratio a focal conic fan texture is observed at 105 °C under crossed Nicols (see Supporting Information). This indicates formation of a Col_h phase. On further cooling, the birefringence disappears entirely following a phase transition to a $Ia\bar{3}d$ Cub_{bi} phase (see Supporting Information). The DSC thermogram of the mixture shows two exothermic peaks at 88 and 43 °C upon cooling (Figure 10). These correspond to the Iso–Col_h and Col_h–Cub_{bi} phase transitions, respectively. The above results show that the ionic LC compounds **2**(10/BF_4) and **5**(10/BF_4) are compatible with lithium salts and form homogeneous mixtures with them.

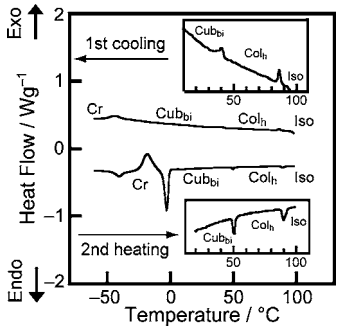

Figure 10. DSC thermograms of the mixture of **5**(10/BF_4)/$LiBF_4$ with a 4:1 molar ratio: Cr, crystalline; Cub_{bi}, bicontinuous cubic; Col_h, hexagonal columnar; Iso, isotropic.

Binary phase diagrams of the mixtures **2**(10/BF_4)/$LiBF_4$ and **5**(10/BF_4)/$LiBF_4$ are presented in Figure 11. It is noteworthy that these ionic compounds maintain the Cub_{bi} phase in the presence of the lithium salts. With increasing mole fraction of the lithium salt, both mixtures show the Col_h phases at temperatures above those of the Cub_{bi} phase. Moreover, the isotropization temperature increases with increasing mole fraction of the lithium salt. These results suggest the following conclusions. One is that the hard lithium cations, being incorporated in the ion channels composed of the ionophilic parts, enhance electrostatic interactions in the ion channels and stabilize the nanosegregated structures. The second conclusion

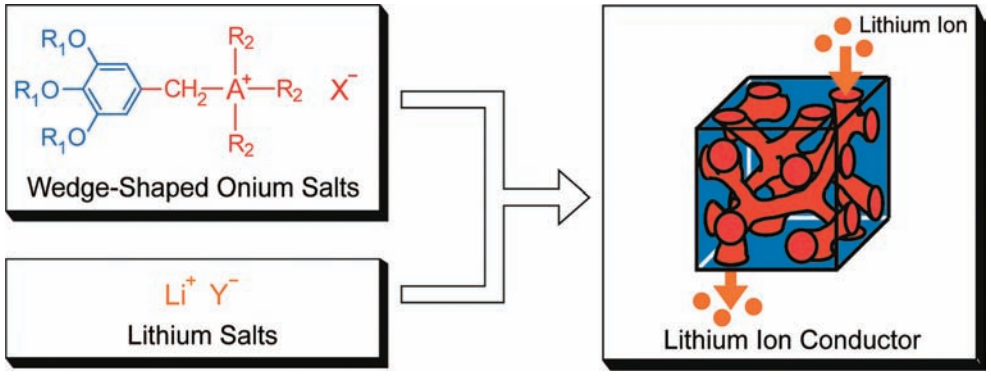

Figure 9. Material design for a new class of lithium ion conductors having a Cub_{bi} LC structure.

dx.doi.org/10.1021/ja209010m | J. Am. Chem.Soc. 2012, 134, 2634–2643

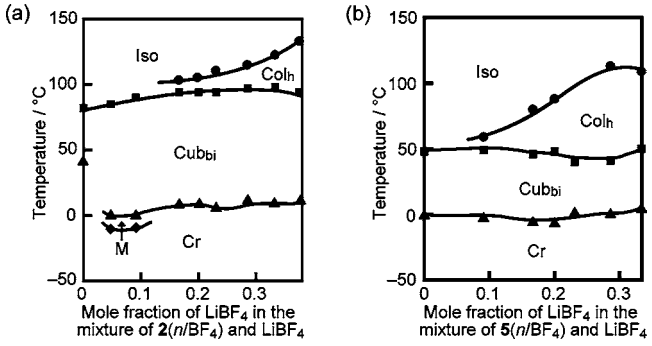

Figure 11. Phase transition temperatures for (a) mixtures of $\mathbf{2}(10/BF_4)$ with $LiBF_4$ and (b) $\mathbf{5}(10/BF_4)$ with $LiBF_4$ on heating as a function of mole fraction of $LiBF_4$: Cr, crystalline; M, unidentified mesophase; Cub_{bi}, bicontinuous cubic; Col_h, hexagonal columnar; Iso, isotropic.

is that the volume balance between the ionophilic and ionophobic parts, which is influenced by the thermal motion and conformation of alkyl chains, significantly affects the mesophase behavior of these materials.

Ionic Conductivities of the LC Materials. Ionic conductivities of the $Ia\bar{3}d$ Cub_{bi} LC materials have been studied by the alternating current impedance method using a comb-shaped gold electrode.[20b] Figure 12 shows the ionic

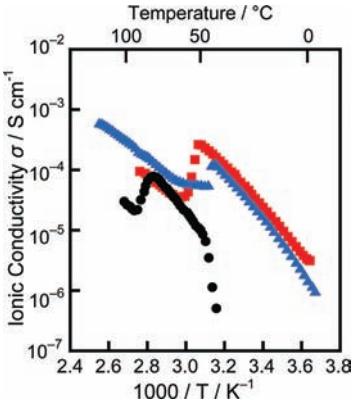

Figure 12. Arrhenius plots of ionic conductivities of ammonium salt $\mathbf{2}(10/BF_4)$ (black circles), phosphonium salt $\mathbf{5}(10/BF_4)$ (red squares), and the complex of phosphonium salt $\mathbf{5}(10/BF_4)$ and $LiBF_4$ with a 4:1 molar ratio (blue triangles).

conductivities of ammonium salt $\mathbf{2}(10/BF_4)$ and phosphonium salt $\mathbf{5}(10/BF_4)$ as a function of temperature. The ionic conductivities for $\mathbf{2}(10/BF_4)$ (black circles) were reported in our preliminary communication.[6] Upon heating, the ionic conductivities for phosphonium salt $\mathbf{5}(10/BF_4)$ (red squares) increase with increasing temperature up to the isotropization temperature. At that temperature the conductivities drop abruptly. We attribute this to the break up of the 3D nanochannel network. This behavior is similar to that of compound $\mathbf{2}(10/BF_4)$. These results further confirm the efficiency of the $Ia\bar{3}d$ Cub_{bi} channel structure for transportation materials. It is noteworthy that phosphonium salt $\mathbf{5}(10/BF_4)$ (red squares) shows higher ionic conductivity than ammonium salt $\mathbf{2}(10/BF_4)$ (black circles) at the same temperature, although the molecular assembled structures formed by $\mathbf{2}(10/BF_4)$ and $\mathbf{5}(10/BF_4)$ are very similar. The highest conductivity achieved for compound $\mathbf{5}(10/BF_4)$ is 2.3×10^{-4} S cm^{-1} at 48 °C, which is about 30 times higher than that of $\mathbf{2}(10/BF_4)$ at the same temperature. The higher ionic conductivities of phosphonium salt $\mathbf{5}(10/BF_4)$ can be explained by the idea that the weaker electrostatic interaction between the phosphonium cationic moiety and the BF_4 anion may form ion channels in which ions can migrate more freely. This explanation is consistent with the known fact that phosphonium-based ionic liquids have lower viscosity and higher ionic conductivity than analogous ammonium-based ionic liquids.[32] It has been established that the difference of the physical properties between phosphonium-based ionic liquids and ammonium-based ionic liquids results from the difference in ionicity between phosphonium and ammonium cations.[31,32] In the case of ionic liquids, it is generally accepted that the weaker the electrostatic interaction within a cation−anion pair is, the lower the viscosity is and the higher ionic conductivity is.[37]

The ionic conductivity of the mixture of $\mathbf{5}(10/BF_4)$ with 0.25 mol of $LiBF_4$ is also plotted against T^{-1} in Figure 12 (blue triangles). The mixture also shows efficient ion conduction in the $Ia\bar{3}d$ Cub_{bi} phase. In this phase the conductivity of the mixture is comparable to that of the single component $\mathbf{5}(10/BF_4)$. Interestingly, above the Cub_{bi}−Col_h transition temperature the ion conductivity of the mixture decreases. For example, the value at 44 °C in the $Ia\bar{3}d$ Cub_{bi} phase is 1.3×10^{-4} S cm^{-1} and that at 50 °C in the Col_h phase is 5.5×10^{-5} S cm^{-1}. The higher ionic conductivity in the $Ia\bar{3}d$ Cub_{bi} phase can be attributed to its 3D channel network structure. In the $Ia\bar{3}d$ Cub_{bi} phase, ions can migrate efficiently through the ion channels even in the presence of structure defects where the channels do not continue because the 3D branched channels in the $Ia\bar{3}d$ Cub_{bi} phase form alternative pathways, bypassing the structure defects. However, in the Col_h phase, the transportation of ions may be blocked by structural defects such as channel ends because ions cannot bypass the defects due to the straight 1D channel structure.

Effect of the Counteranion. For ionic liquids, the counteranions greatly influence their thermal and chemical properties.[38] In order to study the effects of the counteranion on the thermal properties and self-organization behavior of these wedge-shaped ammonium salts, we prepared analogous ammonium salts having other perfluorinated anions, such as PF_6 and CF_3SO_3, which are representative anions for the design of conventional ionic liquids. A comparison of electron density maps for compounds with different anions also allowed us to perform isomorphous replacement X-ray analysis and locate the anions in the structure, as described above (Figure 3b). The thermal properties of compounds $\mathbf{2}(n/PF_6)$ and $\mathbf{2}(n/CF_3SO_3)$ are collected in Table 3. It is apparent that the series of ammonium salts $\mathbf{2}(n/X)$ show some significant differences in phase behavior depending on their anion species.

Figure 13 compares the phase transition behavior of the series of ammonium salts $\mathbf{2}(n/X)$. It is notable that induction of $Ia\bar{3}d$ Cub_{bi} phases is observed in compounds $\mathbf{2}(n/PF_6)$ as well as in $\mathbf{2}(n/BF_4)$. For example, $\mathbf{2}(10/PF_6)$ forms a monotropic $Ia\bar{3}d$ Cub_{bi} phase from 34 to −45 °C. Upon increasing the alkyl chain lengths from 10 to 12, an enantiotropic $Ia\bar{3}d$ Cub_{bi} phase is observed. As the alkyl chains are extended to n = 14 the $Ia\bar{3}d$ Cub_{bi} phase is replaced by the Col_h phase. Compound $\mathbf{2}(14/PF_6)$ forms a Col_h phase from 72 to 114 °C on heating. Such behavior is to be expected, since a larger aliphatic volume increases the effective cross-section at the wide end of the wedge-shaped molecule, thus favoring the Col_h phase. By contrast, $Ia\bar{3}d$ Cub_{bi} phases are favored when the wedge curves

Table 3. Thermal Properties of Ammonium Compounds $2(n/PF_6)$ and $2(n/CF_3SO_3)$

compound	n	phase transition behavior[a]				
$2(n/PF_6)$	10	G	34 (7.7)	Cr	58 (10)	Iso
	12	Cr	64 (48)	Cub_{bi}	76 (0.54)	Iso
	14	Cr	72 (64)	Col_h	114 (0.63)	Iso
$2(n/CF_3SO_3)$	10	Cr	45 (22)	Iso		
	12	Cr	53 (40.4)	Cr	64 (2.6)	Iso
	14	Cr	65 (68)	Iso		

[a]Cr, crystalline; Cub_{bi}, bicontinuous cubic; Col_h, hexagonal columnar; Iso, isotropic. Transition temperatures (°C) and enthalpy changes (kJ mol^{-1}, in parentheses) are determined by DSC on the second heating.

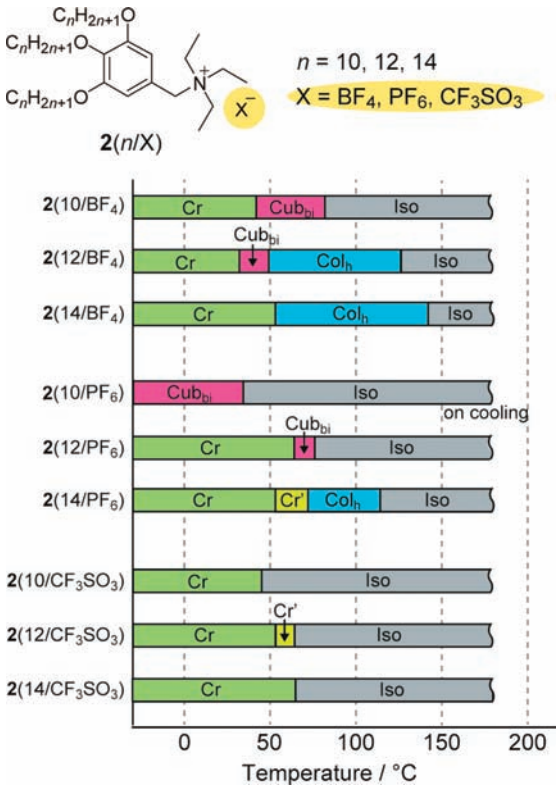

Figure 13. Comparison of LC properties for a series of ammonium salts with different anions: $2(n/BF_4)$, $2(n/PF_6)$, and $2(n/CF_3SO_3)$. Cr, crystalline; Cub_{bi}, bicontinuous cubic; Col_h, hexagonal columnar; Iso, isotropic.

in at the wide end.[3a] In the same fashion the transition from $Ia\bar{3}d$ Cub_{bi} to Col_h phase with increasing temperature can be attributed to the increased wedge cross-section at the wide aliphatic end. On the other hand, compounds $2(n/CF_3SO_3)$, having a bulky anion, never exhibit mesomorphic properties. The bulky anion may sterically disturb their packing into nanosegregated assemblies. Examining the isotropization temperature of compounds $2(n/X)$ it is seen to decrease as the size of the counteranion increases in the order $BF_4 < PF_6 < CF_3SO_3$. For example, the isotropization temperatures of $2(12/BF_4)$, $2(12/PF_6)$, and $2(12/CF_3SO_3)$ are 126, 76, and 64 °C, respectively. The trend is similar to that observed in a series of LC imidazolium salts reported in our previous report.[17] These results suggest that the electrostatic interaction exerts significant effects on the stability of the mesophases.

CONCLUSION

Two series of wedge-shaped ammonium and phosphonium salts have been prepared, and their mesomorphic properties have been successfully examined. These ammonium and phosphonium salts exhibit $Ia\bar{3}d$ Cub_{bi} and Col_h phases depending on the cationic moiety, alkyl chain length n, and anion species. The phase transition behavior of the phosphonium salts is similar to that of the corresponding ammonium salts. To the best of our knowledge, the phosphonium-based compound $5(10/BF_4)$ is the first example of a phosphonium salt showing a thermotropic Cub_{bi} phase, although a few phosphonium salts exhibiting lyotropic Cub_{bi} phases have been reported.[10,33b] The structure of the $Ia\bar{3}d$ Cub_{bi} phase has been further confirmed by electron density mapping based on synchrotron diffraction experiments. Moreover, the location of the anions in the structure has been determined using a novel differential mapping technique. The phase behavior of these salts suggests that the chemical structures of the ionic moiety and alkyl chain length n are important for induction of mesomorphic properties.

Ionic conduction measurements have revealed that the $Ia\bar{3}d$ Cub_{bi} structures with 3D interconnected ion channels are indeed effective in ion transportation. The phosphonium-based Cub_{bi} LC materials show ionic conductivities in the order of 10^{-4} S cm^{-1} at room temperature, which are higher than those of the analogous ammonium-based Cub_{bi} LC materials. The ionic conductivities of conventional amorphous solvent-free solid polymer electrolytes based on poly(ethylene oxide) range from 10^{-8} to 10^{-4} S cm^{-1}.[39] Introduction of well-designed LC nanostructures into these poly(ethylene oxide)-based materials increases the conductivity up to values in the order of 10^{-3} S cm^{-1} at room temperature.[21,26b] On the other hand, for liquid electrolytes, ionic liquids show ionic conductivities ranging from 10^{-3} to 10^{-1} S cm^{-1} at room temperature.[37] Development of solid polymer electrolytes keeping high ionic conductivities using LC nanostructures[7] is our next target.

One of the most interesting aspects of the $Ia\bar{3}d$ Cub_{bi} structures is that their 3D interconnected channels function as transport pathways without the macroscopic orientation of the liquid-crystal domains. In the present study, their application as ion-transporting channels has been demonstrated. However, the utility of these nanochannels may not be limited to ion transportation. Owing to their nano-ordered channel structures, they have great potential to be applied as size-selective filtration membranes. In the near future, the striking innovation of nanochannel materials will be exploited in the development of novel Cub_{bi} LC materials. We believe that the presented research focusing on induction of Cub_{bi} LC phases will help improve the basic knowledge required for designing a new generation of Cub_{bi} LC molecules.

ASSOCIATED CONTENT

Supporting Information

Syntheses, polarizing optical microscopic images, DSC charts, and X-ray diffraction and scattering patterns of compounds **1**–**6**; detailed procedure for construction of the electron density maps for $2(10/BF_4)$, $2(10/PF_6)$, and $5(10/BF_4)$. This material is available free of charge via the Internet at http://pubs.acs.org.

AUTHOR INFORMATION

Corresponding Author

kato@chiral.t.u-tokyo.ac.jp

■ ACKNOWLEDGMENTS

This study was partially supported by the Funding Program for World-Leading Innovative R&D on Science and Technology (FIRST) from the Cabinet Office, Government of Japan, the Global COE Program for Chemistry Innovation through Cooperation of Science and Engineering (T.K.), and a Grant-in-Aid for Scientific Research (A) (No. 19205017) from the Japan Society for the Promotion of Science (JSPS). We also acknowledge support from EC 7th Framework Programme, under contracts NANOGOLD, grant no. 228455. T.I. is grateful for financial support from the JSPS Research Fellowship for Young Scientists and G.U. for support from the WCU program through the National Research Foundation of Korea (R31-10013). For help with the synchrotron experiments we thank Drs. Nick Terrill and Jen Hiller of Diamond Light Source.

■ REFERENCES

(1) Luzzati, V.; Spegt, P. A. *Nature* **1967**, *215*, 701−704.
(2) (a) Bruce, D. W. *Acc. Chem. Res.* **2000**, *33*, 831−840. (b) Kutsumizu, S.; Morita, K.; Ichikawa, T.; Yano, S.; Nojima, S.; Yamaguchi, T. *Liq. Cryst.* **2002**, *29*, 1447−1458. (c) Zeng, X.; Ungar, G.; Impéror-Clerc, M. *Curr. Opin. Colloid Interface Sci.* **2005**, *9*, 370−376.
(3) (a) Zeng, X.; Ungar, G.; Impéror-Clerc, M. *Nat. Mater.* **2005**, *4*, 562−567. (b) Ozawa, K.; Yamamura, Y.; Yasuzuka, S.; Mori, H.; Kutsumizu, S.; Saito, K. *J. Phys. Chem. B* **2008**, *112*, 12179−12181.
(4) (a) Donnio, B.; Heinrich, B.; Gulik-Krzywicki, T.; Delacroix, H.; Guillon, D.; Bruce, D. W. *Chem. Mater.* **1997**, *9*, 2951−2965. (b) Fuchs, P.; Tschierske, C.; Raith, K.; Das, K.; Diele, S. *Angew. Chem., Int. Ed.* **2002**, *41*, 628−631. (c) Ichihara, M.; Suzuki, A.; Hatsusaka, K.; Ohta, K. *Liq. Cryst.* **2007**, *34*, 555−567.
(5) Kato, T. *Angew. Chem., Int. Ed.* **2010**, *49*, 7847−7848.
(6) Ichikawa, T.; Yoshio, M.; Hamasaki, A.; Mukai, T.; Ohno, H.; Kato, T. *J. Am. Chem. Soc.* **2007**, *129*, 10662−10663.
(7) Ichikawa, T.; Yoshio, M.; Hamasaki, A.; Kagimoto, J.; Ohno, H.; Kato, T. *J. Am. Chem. Soc.* **2011**, *133*, 2163−2169.
(8) Frise, A. E.; Ichikawa, T.; Yoshio, M.; Ohno, H.; Dvinskikh, S. V.; Kato, T.; Furó, I. *Chem. Commun.* **2010**, *46*, 728−730.
(9) Lu, X.; Nguyen, V.; Zhou, M.; Zeng, X.; Jin, J.; Elliott, B. J.; Gin, D. L. *Adv. Mater.* **2006**, *18*, 3294−3298.
(10) Zhou, M.; Nemade, P. R.; Lu, X.; Zeng, X.; Hatakeyama, E. S.; Noble, R. D.; Gin, D. L. *J. Am. Chem. Soc.* **2007**, *129*, 9574−9575.
(11) Kerr, R. L.; Miller, S. A.; Shoemaker, R. K.; Elliott, B. J.; Gin, D. L. *J. Am. Chem. Soc.* **2009**, *131*, 15972−15973.
(12) Shah, J. C.; Sadhale, Y.; Chilukuri, D. M. *Adv. Drug Delivery Rev.* **2001**, *47*, 229−250.
(13) Yang, D.; Armitage, B.; Marder, S. R. *Angew. Chem., Int. Ed.* **2004**, *43*, 4402−4409.
(14) (a) Cho, B.-K.; Jain, A.; Gruner, S. M.; Wiesner, U. *Science* **2004**, *305*, 1598−1601. (b) Dobbs, W.; Heinrich, B.; Bourgogne, C.; Donnio, B.; Terazzi, E.; Bonnet, M.-E.; Stock, F.; Erbacher, P.; Bolcato-Bellemin, A.-L.; Douce, L. *J. Am. Chem. Soc.* **2009**, *131*, 13338−13346.
(15) (a) Kato, T.; Mizoshita, N.; Kishimoto, K. *Angew. Chem., Int. Ed.* **2006**, *45*, 38−68. (b) Kato, T. *Science* **2002**, *295*, 2414−2418. (c) Kato, T.; Yasuda, T.; Kamikawa, Y.; Yoshio, M. *Chem. Commun.* **2009**, 729−739.
(16) Kato, T.; Fréchet, J. M. J. *J. Am. Chem. Soc.* **1989**, *111*, 8533−8534.
(17) Yoshio, M.; Ichikawa, T.; Shimura, H.; Kagata, T.; Hamasaki, A.; Mukai, T.; Ohno, H.; Kato, T. *Bull. Chem. Soc. Jpn.* **2007**, *80*, 1836−1841.
(18) (a) Demus, D.; Goodby, J. W.; Gray, G. W.; Spiess, H.-W.; Vill, V. *Handbook of Liquid Crystals*; Wiley-VCH: Weinheim, Germany, 1998. (b) Tschierske, C. *J. Mater. Chem.* **1998**, *8*, 1485−1508. (c) Hudson, S. D.; Jung, H.-T.; Percec, V.; Cho, W.-D.; Johansson, G.; Ungar, G.; Balagurusamy, V. S. K. *Science* **1997**, *278*, 449−452. (d) Gin, D. L.; Gu, W.; Pindzola, B. A.; Zhou, W.-J. *Acc. Chem. Res.* **2001**, *34*, 973−980. (e) Seddon, J. M.; Robins, J.; Gulik-Krzywicki, T.; Delacroix, H. *Phys. Chem. Chem. Phys.* **2000**, *2*, 4485−4493. (f) Bisoyi, H. K.; Kumar, S. *Chem. Soc. Rev.* **2010**, *39*, 264−285. (g) Saez, I. M.; Goodby, J. W. *J. Mater. Chem.* **2005**, *15*, 26−40. (h) Ungar, G.; Liu, Y.; Zeng, X.; Percec, V.; Cho, W.-D. *Science* **2003**, *299*, 1208−1211.
(19) (a) Chen, B.; Baumeister, U.; Pelzl, G.; Das, M. K.; Zeng, X.; Ungar, G.; Tschierske, C. *J. Am. Chem. Soc.* **2005**, *127*, 16578−16591. (b) Percec, V.; Holerca, M. N.; Uchida, S.; Cho, W.-D.; Ungar, G.; Lee, Y.; Yeardley, D. J. P. *Chem.—Eur. J.* **2002**, *8*, 1106−1117. (c) Choi, J.-W.; Ryu, M.-H.; Lee, E.; Cho, B.-K. *Chem.—Eur. J.* **2010**, *16*, 9006−9009. (d) Jin, L. Y.; Bae, J.; Ryu, J.-H.; Lee, M. *Angew. Chem., Int. Ed.* **2006**, *45*, 650−653.
(20) (a) Yoshio, M.; Mukai, T.; Kanie, K.; Yoshizawa, M.; Ohno, H.; Kato, T. *Adv. Mater.* **2002**, *14*, 351−354. (b) Yoshio, M.; Mukai, T.; Ohno, H.; Kato, T. *J. Am. Chem. Soc.* **2004**, *126*, 994−995. (c) Kato, T.; Yoshio, M. In *Electrochemical Aspects of Ionic Liquids*; Ohno, H., Ed.; Wiley: Hoboken, NJ, 2005; Chapter 25, pp 307−320. (d) Yoshio, M.; Kagata, T.; Hoshino, K.; Mukai, T.; Ohno, H.; Kato, T. *J. Am. Chem. Soc.* **2006**, *128*, 5570−5577. (e) Shimura, H.; Yoshio, M.; Hoshino, K.; Mukai, T.; Ohno, H.; Kato, T. *J. Am. Chem. Soc.* **2008**, *130*, 1759−1765. (f) Yoshio, M.; Mukai, T.; Ohno, H.; Kato, T. *ACS Symp. Ser.* **2007**, *975*, 161−171.
(21) Kishimoto, K.; Suzawa, T.; Yokota, T.; Mukai, T.; Ohno, H.; Kato, T. *J. Am. Chem. Soc.* **2005**, *127*, 15618−15623.
(22) Yasuda, T.; Ooi, H.; Morita, J.; Akama, Y.; Minoura, K.; Funahashi, M.; Shimomura, T.; Kato, T. *Adv. Funct. Mater.* **2009**, *19*, 411−419.
(23) (a) Simpson, C. D.; Wu, J.; Watson, M. D.; Müllen, K. *J. Mater. Chem.* **2004**, *14*, 494−504. (b) Funahashi, M.; Zhang, F.; Tamaoki, N. *Adv. Mater.* **2007**, *19*, 353−358. (c) Percec, V.; Glodde, M.; Bera, T. K.; Miura, Y.; Shiyanovskaya, I.; Singer, K. D.; Balagurusamy, V. S. K.; Helney, P. A.; Schnell, I.; Rapp, A.; Spiess, H.-W.; Hudson, S. D.; Duan, H. *Nature* **2002**, *419*, 384−387. (d) Boden, N.; Bushby, R. J.; Clements, J.; Movaghar, B. *J. Mater. Chem.* **1999**, *9*, 2081−2086.
(24) Yazaki, S.; Funahashi, M.; Kagimoto, J.; Ohno, H.; Kato, T. *J. Am. Chem. Soc.* **2010**, *132*, 7702−7708.
(25) Sagara, Y.; Kato, T. *Nat. Chem.* **2009**, *1*, 605−610.
(26) (a) Ikkala, O.; ten Brinke, G. *Chem. Commun.* **2004**, 2131−2137. (b) Zheng, Y.; Lui, J.; Ungar, G.; Wright, P. V. *Chem. Rec.* **2004**, *4*, 176−191.
(27) (a) Binnemans, K. *Chem. Rev.* **2005**, *105*, 4148−4204. (b) Bazuin, C. G.; Guillon, D.; Skoulios, A.; Nicoud, J.-F. *Liq. Cryst.* **1986**, *1*, 181−188. (c) Ujiie, S.; Iimura, K. *Chem. Lett.* **1990**, 995−998. (d) Kosaka, Y.; Kato, T.; Uryu, T. *Liq. Cryst.* **1995**, *18*, 693−698. (e) Bravo-Grimaldo, E.; Navarro-Rodríguez, D.; Skoulios, A.; Guillon, D. *Liq. Cryst.* **1996**, *20*, 393−398. (f) Gordon, C. M.; Holbrey, J. D.; Kennedy, A. R.; Seddon, K. R. *J. Mater. Chem.* **1998**, *8*, 2627−2636. (g) Kouwer, P. H. J.; Swager, T. M. *J. Am. Chem. Soc.* **2007**, *129*, 14042−14052.
(28) (a) Neve, F.; Impéror-Clerc, M. *Liq. Cryst.* **2004**, *31*, 907−912. (b) Boydston, A. J.; Pecinovsky, C. S.; Chao, S. T.; Bielawski, C. W. *J. Am. Chem. Soc.* **2007**, *129*, 14550−14551. (c) Alam, M. A.; Motoyanagi, J.; Yamamoto, Y.; Fukushima, T.; Kim, J.; Kato, K.; Takata, M.; Saeki, A.; Seki, S.; Tagawa, S.; Aida, T. *J. Am. Chem. Soc.* **2009**, *131*, 17722−17723.
(29) Hatakeyama, E. S.; Wiesenauer, B. R.; Gabriel, C. J.; Noble, R. D.; Gin, D. L. *Chem. Mater.* **2010**, *22*, 4525−4527.
(30) (a) Arce, A.; Earle, M. J.; Katdare, S. P.; Rodríguez, H.; Seddon, K. R. *Chem. Commun.* **2006**, 2548−2550. (b) Fukumoto, K.; Ohno, H. *Angew. Chem., Int. Ed.* **2007**, *46*, 1852−1855.
(31) Vega, J. A.; Zhou, J.; Kohl, P. A. *J. Electrochem. Soc.* **2009**, *156*, A253−A259.
(32) Seki, S.; Hayamizu, K.; Tsuzuki, S.; Fujii, K.; Umebayashi, Y.; Mitsugi, T.; Kobayashi, T.; Ohno, Y.; Kobayashi, Y.; Mita, Y.; Miyashiro, H.; Ishiguro, S. *Phys. Chem. Chem. Phys.* **2009**, *11*, 3509−3514.

(33) (a) Kanazawa, A.; Ikeda, T.; Abe, J. *J. Am. Chem. Soc.* **2001**, *123*, 1748−1754. (b) Pindzola, B. A.; Jin, J.; Gin, D. L. *J. Am. Chem. Soc.* **2003**, *125*, 2940−2949.
(34) Abdallah, D. J.; Robertson, A.; Hsu, H.-F.; Weiss, R. G. *J. Am. Chem. Soc.* **2000**, *122*, 3053−3062.
(35) Dukeson, D. R.; Ungar, G.; Balagurusamy, V. S. K.; Percec, V.; Johansson, G.; Glodde, M. *J. Am. Chem. Soc.* **2003**, *125*, 15974−15980.
(36) Ungar, G.; Percec, V.; Holerca, M. N.; Johansson, G.; Heck, J. A. *Chem.—Eur. J.* **2000**, *6*, 1258−1266.
(37) (a) Pringle, J. M.; Golding, J.; Forsyth, C. M.; Deacon, G. B.; Forsyth, M.; MacFarlane, D. R. *J. Mater. Chem.* **2002**, *12*, 3475−3480. (b) Ohno, H. *Bull. Chem. Soc. Jpn.* **2006**, *79*, 1665−1680. (c) Tokuda, H.; Tsuzuki, S.; Susan, M. A. B. H.; Hayamizu, K.; Watanabe, M. *J. Phys. Chem. B* **2006**, *110*, 19593−19600.
(38) (a) Armand, M.; Endres, F.; MacFarlane, D. R.; Ohno, H.; Scrosati, B. *Nat. Mater.* **2009**, *8*, 621−629. (b) Wasserscheid, P.; Keim, W. *Angew. Chem., Int. Ed.* **2000**, *39*, 3772−3789.
(39) Meyer, W. H. *Adv. Mater.* **1998**, *10*, 439−448.